

Received:  
29 November 2013

Revised:  
6 February 2014

Accepted:  
19 February 2014

doi: 10.1259/bjr.20130780

Cite this article as:

Codreanu I, Robson MD, Rider OJ, Pegg TJ, Dasanu CA, Jung BA, et al. Details of left ventricular radial wall motion supporting the ventricular theory of the third heart sound obtained by cardiac MR. *Br J Radiol* 2014;87:20130780.

## FULL PAPER

# Details of left ventricular radial wall motion supporting the ventricular theory of the third heart sound obtained by cardiac MR

<sup>1,2</sup>I CODREANU, MD, PhD, <sup>3</sup>M D ROBSON, PhD, <sup>3</sup>O J RIDER, BMBCh, DPhil, <sup>3</sup>T J PEGG, MB ChB, DPhil, <sup>4</sup>C A DASANU, MD, PhD, <sup>5,6</sup>B A JUNG, PhD, <sup>2</sup>N ROTARU, MD, PhD, <sup>1</sup>K CLARKE, MA, PhD and <sup>1,2,7</sup>C J HOLLOWAY, MRCP, DPhil

<sup>1</sup>Department of Physiology, Anatomy and Genetics, University of Oxford, Oxford, UK

<sup>2</sup>Department of Radiology, Medpark International Hospital, State University of Medicine and Pharmacy "Nicolae Testemitanu", Chisinau, Moldova

<sup>3</sup>Radcliffe Department of Medicine, University of Oxford Centre for Clinical Magnetic Resonance Research, Oxford, UK

<sup>4</sup>Department of Hematology-Oncology, Saint Francis Hospital and Medical Center, University of Connecticut, Hartford, CT, USA

<sup>5</sup>Department of Diagnostic Radiology, Medical Physics, University Hospital, Freiburg, Germany

<sup>6</sup>Institute of Diagnostic, Interventional and Pediatric Radiology, University Hospital, Bern, Switzerland

<sup>7</sup>Department of Cardiology, St Vincent's Hospital, Darlinghurst, NSW, Australia

Address correspondence to: Dr Ion Codreanu

E-mail: [codrion@yahoo.com](mailto:codrion@yahoo.com)

**Objective:** Obtaining new details of radial motion of left ventricular (LV) segments using velocity-encoding cardiac MRI.

**Methods:** Cardiac MR examinations were performed on 14 healthy volunteers aged between 19 and 26 years. Cine images for navigator-gated phase contrast velocity mapping were acquired using a black blood segmented  $k$ -space spoiled gradient echo sequence with a temporal resolution of 13.8 ms. Peak systolic and diastolic radial velocities as well as radial velocity curves were obtained for 16 ventricular segments.

**Results:** Significant differences among peak radial velocities of basal and mid-ventricular segments have been recorded. Particular patterns of segmental radial velocity curves were also noted. An additional wave of outward radial movement during the phase of rapid ventricular filling, corresponding to the expected timing of the third heart sound, appeared of particular interest.

**Conclusion:** The technique has allowed visualization of new details of LV radial wall motion. In particular, higher peak systolic radial velocities of anterior and inferior segments are suggestive of a relatively higher dynamics of anteroposterior vs lateral radial motion in systole. Specific patterns of radial motion of other LV segments may provide additional insights into LV mechanics.

**Advances in knowledge:** The outward radial movement of LV segments impacted by the blood flow during rapid ventricular filling provides a potential substrate for the third heart sound. A biphasic radial expansion of the basal anteroseptal segment in early diastole is likely to be related to the simultaneous longitudinal LV displacement by the stretched great vessels following repolarization and their close apposition to this segment.

Advances in cardiac imaging techniques have allowed evaluation of new details of the complex pattern of left ventricular (LV) motion. Using high temporal resolution cardiovascular MR with myocardial velocity-encoding techniques, we previously performed a detailed analysis of rotational and longitudinal motions of the left ventricle, correlating them with the orientation or cardiomyocyte aggregates within the LV wall.<sup>1,2</sup> However, accurate evaluation of radial motion is equally important. For example, radial wall motion abnormalities have been detected in patients with diabetes<sup>3</sup> and hypertrophic cardiomyopathy,<sup>4</sup> whereas radial dyssynchrony is almost universal in patients with heart failure.<sup>5</sup> The purpose of this study was to obtain new details of global and regional radial wall motion of the

left ventricle using the cardiac MR high temporal resolution myocardial velocity-encoding technique.<sup>6,7</sup> Considering recent interest in myocardial multilayer measurements, which provide more layer-specific information about the functional state of the myocardium at different levels,<sup>8-13</sup> separate calculations of all myocardial velocities and their corresponding peak times for the inner (endocardial), middle (transmural) and outer (epicardial) layers of the LV wall were performed.

## METHODS AND MATERIALS

### Subjects and imaging

Cardiac MR examinations with myocardial velocity encoding were performed on 14 volunteers aged between 19 and 26 years. All subjects were athletic healthy male volunteers

Table 1. Peak systolic and diastolic radial velocities for axial left ventricular (LV) slices included in the study

Velocities	LV base (Segments 1–6)	Mid-LV level (Segments 7–12)	LV apex (Segments 13–16)	<i>p</i> -value
Peak systolic velocity ( $\text{cm s}^{-1}$ )				
Epicardial	$3.0 \pm 0.2$	$3.2 \pm 0.1$	$2.6 \pm 0.2$	0.014
Transmural	$3.5 \pm 0.2$	$3.7 \pm 0.1$	$3.1 \pm 0.2$	0.015
Endocardial	$4.0 \pm 0.2$	$4.2 \pm 0.1$	$3.6 \pm 0.2$	0.025
Peak diastolic velocity ( $\text{cm s}^{-1}$ )				
Epicardial	$-4.5 \pm 0.3$	$-4.6 \pm 0.2$	$-4.9 \pm 0.3$	0.510
Transmural	$-5.5 \pm 0.3$	$-5.6 \pm 0.3$	$-5.8 \pm 0.4$	0.730
Endocardial	$-6.6 \pm 0.4$	$-6.6 \pm 0.3$	$-6.9 \pm 0.5$	0.880

One-way analysis of variance was used to test for differences among means (values are mean  $\pm$  standard error of mean).

with no history of smoking or cardiovascular disease. Their baseline characteristics included a body mass index of  $24 \pm 2 \text{ kg m}^{-2}$  (mean  $\pm$  standard deviation), a heart rate of  $57 \pm 7$  beats per minute, a systolic blood pressure of  $119 \pm 8 \text{ mmHg}$ , a diastolic blood pressure of  $75 \pm 4 \text{ mmHg}$  and an LV ejection fraction of  $68 \pm 6$ . The study was conducted according to the principles of the Declaration of Helsinki and was approved by a local Oxfordshire clinical research ethics committee. Each subject provided written informed consent.

The cardiac MR scans were performed using a 1.5-T Siemens Sonata clinical scanner (Siemens Healthcare, Erlangen, Germany). Pilot images, followed by horizontal and vertical long axis cine images, were acquired using a steady-state free precession pulse sequence. Cine images for navigator-gated high temporal resolution phase contrast velocity mapping were acquired using a black blood segmented  $\kappa$ -space spoiled gradient echo sequence<sup>6,7</sup> with a temporal resolution of 13.8 ms (repetition time = 13.8 ms, echo time = 5.0 ms, flip angle =  $15^\circ$ , bandwidth = 650 Hz per pixel, field of view =  $400 \times 300 \text{ mm}$  and matrix =  $256 \times 96$ ).<sup>1,2</sup> Three short axis images were acquired for the LV base, mid-ventricle and apex. The basal slice was positioned parallel to the base of the heart and distal to the LV outflow tract. Basal, mid-ventricular and apical slices were positioned 15–20 mm apart, depending on the heart size. With cardiac and respiratory gating, each short axis acquisition took approximately 3–5 min, with an average of 60–70 phases per cardiac cycle. Velocity encoding was performed by including a phase image with no velocity encoding followed by images with a bipolar gradient in the read, phase or slice direction after each radiofrequency pulse to the otherwise identical sequence [velocity-encoded gradient echo imaging (VENC) in-plane =  $20 \text{ cm s}^{-1}$ , VENC through-plane =  $30 \text{ cm s}^{-1}$ ]. Post-processing was performed in the standard fashion of subtracting the phase from the image with no velocity encoding, followed by conversion of the phase data into velocity maps. Separate measurements were performed for the inner (endocardial) and outer (epicardial) layers. Transmural peak velocities were inferred automatically as averaged peak values of the inner and outer layers. The duration of the cardiac cycle was determined by the R–R interval on the electrocardiogram, with end systole defined as the smallest LV cavity. The cardiac phases were subsequently

calculated and normalized for the entire group based on their average duration during a cardiac cycle.<sup>2,14,15</sup>

Tissue phase mapping (TPM) analysis was performed using customized software (MATLAB® v. 6.5; MathWorks®, Natick, MA). For TPM analysis, the left ventricle was divided into 16 segments (6 basal, 6 middle and 4 apical) according to the American Heart Association (AHA) model.<sup>16</sup> The endocardial and epicardial borders were manually contoured for basal, mid-ventricular and apical segments for each phase of the cardiac cycle. In-plane velocities were transformed into an internal polar coordinate system positioned at the centre of the mass of the left ventricle. Global ventricular velocity time courses for radial motion of all LV segments were calculated by averaging over the entire segmentation mask as well as the corresponding peak radial velocities and time to peak. Graphical representations of radial velocities during a cardiac cycle for individual LV segments were also obtained.

### Statistical analysis

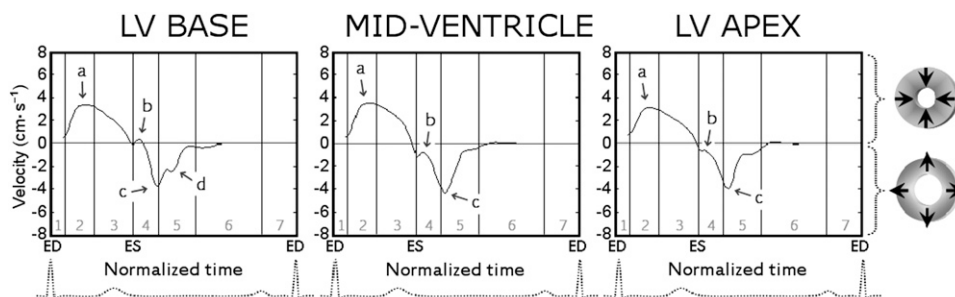
MATLAB files containing TPM data were converted and generated into Microsoft Excel™ (Microsoft Corporation, Redmond, WA) files for statistical analysis. Subsequently, all data were analysed using SPSS® v. 16.0 (SPSS Inc., Chicago, IL) and MedCalc® statistical software v. 12.5.0 (MedCalc Software, Ostend, Belgium). Radial velocities were expressed as continuous variables and tested for normal distribution. One-way analysis of variance (ANOVA) was used to test for differences among mean rotational velocities of individual LV segments. Before the ANOVA test, Levene's test for equality of variances was performed to ensure that the variables obtained for the compared segments were homogeneous (a standard function of MedCalc software). If the ANOVA test was positive ( $p < 0.05$ ), a *post hoc* Scheffé test was performed to identify sample means that were significantly different from each other.

### RESULTS

Average radial velocities for basal, mid-ventricular and apical segments

Peak systolic and diastolic radial velocities for basal, mid-ventricular and apical segments are presented in Table 1. Positive values reflect ventricular wall movement towards the centre of

Figure 1. Radial velocity graphs for axial left ventricular (LV) slices included in the study. The curves represent average values for all segments at the respective LV level. Positive values reflect inward motion towards the centre of the ventricle, whereas negative values show outward expansion. The arrows show peak systolic radial velocity (a), an upright directed notch in early diastole (b), peak diastolic radial velocity (c) and an additional wave of outward radial movement during rapid ventricular filling (d). Cardiac cycle phases: 1, isovolumetric contraction; 2, rapid ejection; 3, reduced ejection; 4, isovolumetric relaxation; 5, rapid filling; 6, diastasis; and 7, atrial systole. ED, end diastole; ES, end systole.



the ventricle and negative values show an outward movement (Figure 1). Both systolic and diastolic peak velocities increased incrementally from the epicardium towards the endocardium. Lower peak systolic velocities have been recorded for the apical LV slice, the difference between means reaching a 5% significance level for all layers ( $p < 0.05$ ). The *post hoc* Scheffé test for pairwise comparisons confirmed significant differences between the mean values of peak systolic radial

velocities recorded for apical compared with mid-ventricular segments ( $p < 0.05$ ). No significant differences were noted between the average values of peak diastolic radial velocities recorded for basal, mid-ventricular and apical segments (Table 1).

The variation in radial velocities during a cardiac cycle at different LV levels is shown in Figure 1. Little radial

Figure 2. Radial velocity graphs for basal left ventricular segments during a cardiac cycle. The graphs represent the average myocardial velocities for all volunteers. Positive values reflect inward motion towards the centre of the ventricle, whereas negative values show outward expansion. The arrows show peak systolic radial velocity (a), an upright directed notch in early diastole (b), peak diastolic radial velocity (c) and an additional wave of outward radial movement during rapid ventricular filling (d). Of note is that, in Segment 2, the peak diastolic radial velocity was delayed and represented by the second wave of radial expansion (d). Segments: 1, basal anterior segment; 2, basal anteroseptal segment; 3, basal inferoseptal segment; 4, basal inferior segment; 5, basal inferolateral segment; and 6, basal anterolateral segment. Cardiac cycle phases: 1, isovolumetric contraction; 2, rapid ejection; 3, reduced ejection; 4, isovolumetric relaxation; 5, rapid filling; 6, diastasis; and 7, atrial systole. ED, end diastole; ES, end systole.

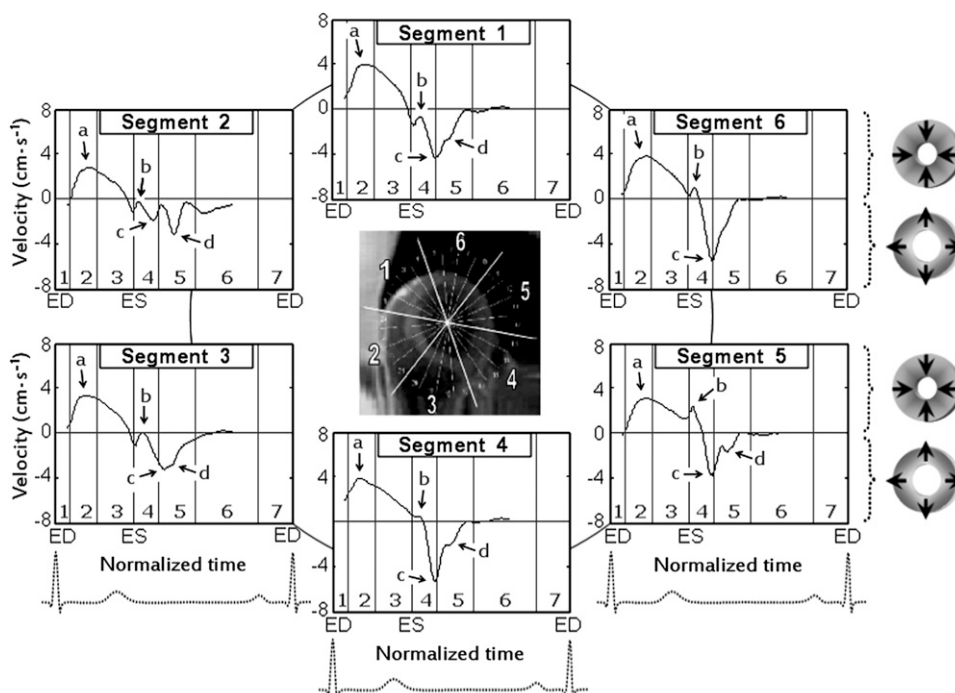


Table 2. Peak systolic and diastolic radial velocities for basal left ventricular segments<sup>a</sup>

Velocities	Segment 1	Segment 2	Segment 3	Segment 4	Segment 5	Segment 6	<i>p</i> -value
Peak systolic velocity (cm s <sup>-1</sup> )							
Epicardial	4.8 ± 0.3	3.4 ± 0.3	4.1 ± 0.3	5.1 ± 0.3	3.6 ± 0.2	3.7 ± 0.3	<0.001
Transmural	5.0 ± 0.3	3.6 ± 0.3	4.4 ± 0.3	5.1 ± 0.3	3.9 ± 0.2	4.1 ± 0.2	<0.001
Endocardial	5.4 ± 0.3	4.0 ± 0.2	4.9 ± 0.3	5.3 ± 0.2	4.5 ± 0.2	4.6 ± 0.2	<0.001
Peak diastolic velocity (cm s <sup>-1</sup> )							
Epicardial	-5.1 ± 0.4	-5.9 ± 0.6	-4.9 ± 0.3	-6.9 ± 0.6	-5.4 ± 0.4	-6.8 ± 0.5	0.029
Transmural	-6.1 ± 0.5	-6.3 ± 0.6	-6.1 ± 0.3	-8.2 ± 0.6	-6.8 ± 0.4	-8.0 ± 0.5	0.002
Endocardial	-7.1 ± 0.6	-6.8 ± 0.6	-7.6 ± 0.4	-9.7 ± 0.7	-8.5 ± 0.6	-9.2 ± 0.6	<0.001

<sup>a</sup>One-way analysis of variance was used to test for differences among means (values are mean ± standard error of mean).

movement occurred during isovolumetric contraction, the velocity curve remaining close to baseline at the end of this phase. A subsequent rapid increase in radial velocity, peaking by the middle of rapid ejection (Figure 1, wave a), was followed by a gradual decrease of LV inward movement during the phase of reduced ventricular ejection. A small upward directed notch at the beginning of diastole (Figure 1, wave b) was consistent with a brief moment of deceleration in the radial expansion at the beginning of isovolumetric relaxation. The outward radial movement in diastole reached peak velocity values by the end of isovolumetric relaxation and

beginning of rapid ventricular filling (Figure 1, wave c). An additional wave of outward radial motion was noted at the LV base during the phase of rapid ventricular filling (Figure 1, wave d), corresponding to the expected timing of the third heart sound. By the end of rapid ventricular filling (Phase 5), the velocity curve returned to baseline and little radial movement was noted after the ventricle was filled (Figure 1, Phase 6). Another wave of outward radial motion may be expected during atrial contraction (Figure 1, Phase 7); however, TPM acquisition was prospectively gated and the effect of atrial contraction on LV filling was not visualized.

Figure 3. Radial velocity graphs for mid-ventricular segments during a cardiac cycle. The graphs represent the average myocardial velocities for all volunteers. Positive values reflect inward motion towards the centre of the ventricle, whereas negative values show outward expansion. The arrows show peak systolic radial velocity (a), an upright directed notch in early diastole (b), peak diastolic radial velocity (c) and an additional wave of outward radial movement during rapid ventricular filling (d). Segments: 7, mid-anterior segment; 8, mid-anterosseptal segment; 9, mid-inferoseptal segment; 10, mid-inferior segment; 11, mid-inferolateral segment; and 12, mid-antrolateral segment. Cardiac cycle phases: 1, isovolumetric contraction; 2, rapid ejection; 3, reduced ejection; 4, isovolumetric relaxation; 5, rapid filling; 6, diastasis; and 7, atrial systole. ED, end diastole; ES, end systole.

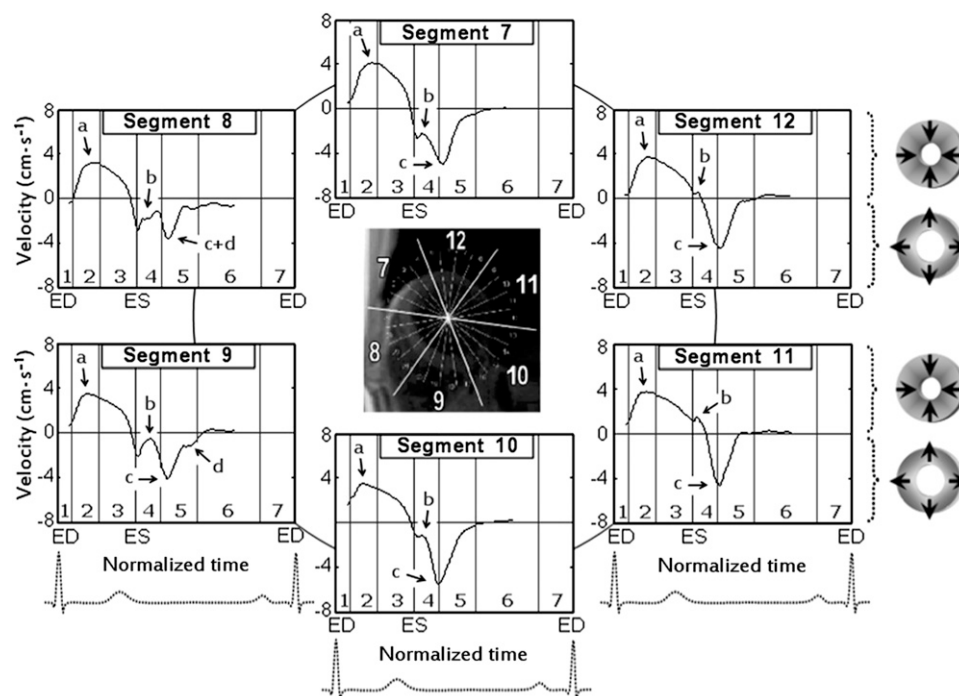


Table 3. Peak systolic and diastolic radial velocities for mid-ventricular segments<sup>a</sup>

Velocities	Segment 7	Segment 8	Segment 9	Segment 10	Segment 11	Segment 12	p-value
Peak systolic velocity ( $\text{cm s}^{-1}$ )							
Epicardial	$4.6 \pm 0.4$	$3.0 \pm 0.2$	$3.6 \pm 0.2$	$5.1 \pm 0.4$	$4.1 \pm 0.3$	$3.4 \pm 0.2$	$<0.001$
Transmural	$5.0 \pm 0.4$	$3.5 \pm 0.2$	$3.9 \pm 0.2$	$5.3 \pm 0.4$	$4.4 \pm 0.3$	$3.9 \pm 0.2$	$<0.001$
Endocardial	$5.4 \pm 0.4$	$4.1 \pm 0.2$	$4.4 \pm 0.2$	$5.6 \pm 0.3$	$4.9 \pm 0.3$	$4.4 \pm 0.2$	0.001
Peak diastolic velocity ( $\text{cm s}^{-1}$ )							
Epicardial	$-5.8 \pm 0.4$	$-5.6 \pm 0.4$	$-5.6 \pm 0.4$	$-6.6 \pm 0.6$	$-4.9 \pm 0.3$	$-4.9 \pm 0.3$	0.031
Transmural	$-6.8 \pm 0.4$	$-6.2 \pm 0.4$	$-6.5 \pm 0.4$	$-7.7 \pm 0.5$	$-6.1 \pm 0.3$	$-6.1 \pm 0.3$	0.059
Endocardial	$-8.0 \pm 0.4$	$-7.1 \pm 0.5$	$-7.6 \pm 0.5$	$-8.8 \pm 0.5$	$-7.6 \pm 0.4$	$-7.4 \pm 0.3$	0.107

<sup>a</sup>One-way analysis of variance was used to test for differences among means (values are mean  $\pm$  standard error of mean).

### Radial velocities of basal left ventricular segments

The variation in radial velocities during a cardiac cycle for basal LV segments is shown in Figure 2. In all basal LV segments, peak systolic velocity values were reached during the phase of rapid ejection (Figure 2, wave a), after which the velocity of the inward radial movement gradually decreased until the end of systole. A delay in the commencement of radial expansion was noted in the basal inferolateral segment (*i.e.* Segment 5), its radial velocity curve remaining well above zero at the end of systole and showing no outward radial expansion until the second half of isovolumetric relaxation (Figure 2). A rather unusual pattern of radial expansion was recorded in the basal anteroseptal segment

(*i.e.* Segment 2), which showed a biphasic shape of outward radial motion in diastole (Figure 2, Segment 2, waves c and d). Of note is that the peak diastolic radial velocity in this segment was significantly delayed and represented by the second wave of radial expansion (Figure 2, Segment 2, wave d), which was in contrast to the rest of the LV segments. A related delay in reaching peak diastolic velocity values was also noted in the adjacent basal inferoseptal segment (Figure 2, Segment 3, wave c). An additional wave of outward radial motion during the phase of rapid ventricular filling, corresponding to the expected timing of the third heart sound, was apparent in most segments (Figure 2, wave d). By the end of rapid ventricular filling (Phase 5), the

Figure 4. Radial velocity graphs for apical left ventricular segments during a cardiac cycle. The graphs represent the average myocardial velocities for all volunteers. Positive values reflect inward motion towards the centre of the ventricle, whereas negative values show outward expansion. The arrows show peak systolic radial velocity (a), an upright directed notch in early diastole (b) and peak diastolic radial velocity (c). Segments: 13, apical anterior segment; 14, apical septal segment; 15, apical inferior segment; and 16, apical lateral segment. Cardiac cycle phases: 1, isovolumetric contraction; 2, rapid ejection; 3, reduced ejection; 4, isovolumetric relaxation; 5, rapid filling; 6, diastasis; and 7, atrial systole. ED, end diastole; ES, end systole.

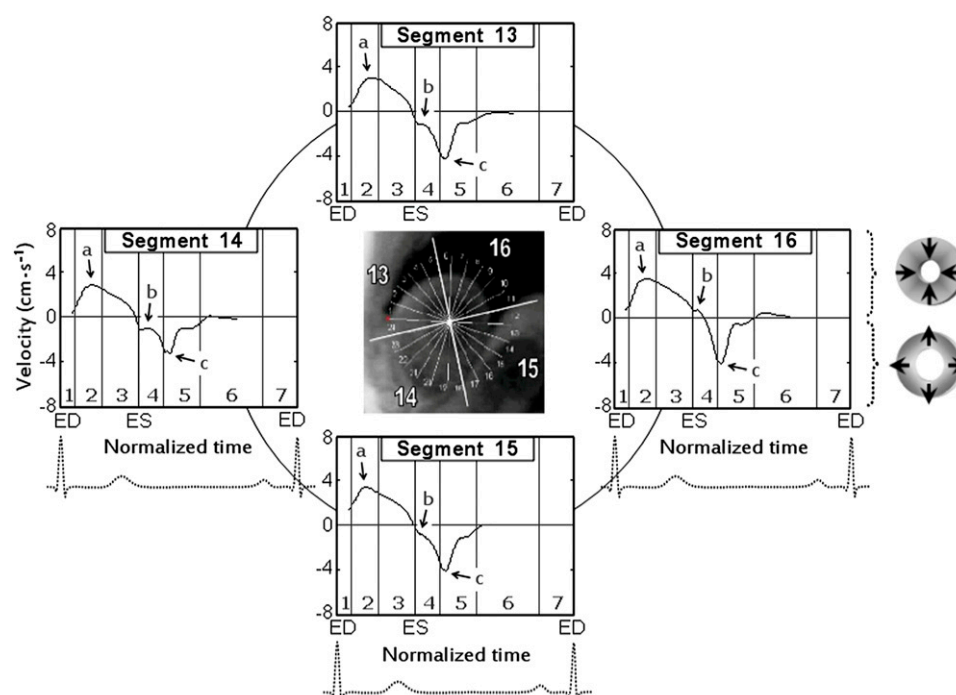




Table 4. Peak systolic and diastolic radial velocities for apical left ventricular segments<sup>a</sup>

Velocities	Segment 13	Segment 14	Segment 15	Segment 16	p-value
Peak systolic velocity (cm s <sup>-1</sup> )					
Epicardial	3.1 ± 0.3	2.6 ± 0.3	3.2 ± 0.2	3.1 ± 0.2	0.331
Transmural	3.4 ± 0.3	3.0 ± 0.3	3.6 ± 0.2	3.5 ± 0.2	0.314
Endocardial	3.9 ± 0.3	3.5 ± 0.3	4.1 ± 0.2	4.2 ± 0.1	0.177
Peak diastolic velocity (cm s <sup>-1</sup> )					
Epicardial	-5.0 ± 0.3	-5.4 ± 0.4	-5.3 ± 0.3	-5.6 ± 0.4	0.315
Transmural	-6.0 ± 0.4	-6.0 ± 0.5	-6.3 ± 0.3	-6.8 ± 0.4	0.675
Endocardial	-7.0 ± 0.4	-6.8 ± 0.5	-7.3 ± 0.4	-8.1 ± 0.5	0.263

<sup>a</sup>One-way analysis of variance was used to test for differences among means (values are mean ± standard error of mean).

velocity of the radial expansion decreased in all basal LV segments and little radial movement occurred in Phase 6 (diastasis).

The peak systolic and diastolic radial velocities of basal LV segments are provided in Table 2. The *post hoc* Scheffé test showed significant differences ( $p < 0.05$ ) between peak systolic velocities recorded in the following segments: 1 vs 2, 3; 2 vs 1, 4; 3 vs 1; and 4 vs 2 for the inner (endocardial); 1 vs 2, 3; 2 vs 1, 4; 3 vs 1, 4; 4 vs 2, 3, 5; and 5 vs 4 for the middle (transmural); and

1 vs 2, 3; 2 vs 1, 4; 3 vs 1, 4; 4 vs 2, 3, 5, 6; 5 vs 4; and 6 vs 4 for the outer (epicardial) layers as well as between peak diastolic velocities recorded in the following segments: 2 vs 4; 3 vs 4, 6; 4 vs 2, 3; and 6 vs 3 for the inner (endocardial) layer and 3 vs 4 for the middle (transmural) layer.

#### Radial velocities of mid-ventricular segments

The radial velocity graphs for mid-ventricular segments during a cardiac cycle are shown in Figure 3. In all mid-ventricular

Figure 5. Schematic representation of left ventricular segments on the cross-section and radial velocity curves for Segments 2, 5 and 8. The arrows show peak systolic radial velocity (a), an upright directed notch in early diastole (b) and peak diastolic radial velocity (c). An additional wave of outward radial movement during rapid ventricular filling (d) was noted in ventricular segments that are likely to be particularly influenced by ventricular filling because of the direction of blood flow through the mitral valve. This wave is strongly supporting the ventricular theory of the third heart sound. Segments: 2, basal anteroseptal segment; 5, basal inferolateral segment; 8, mid-anteroseptal segment; 11, mid-inferolateral segment; 14, apical septal segment; and 16, apical lateral segment. Cardiac cycle phases: 1, isovolumetric contraction; 2, rapid ejection; 3, reduced ejection; 4, isovolumetric relaxation; 5, rapid filling; 6, diastasis; and 7, atrial systole. ED, end diastole; ES, end systole.

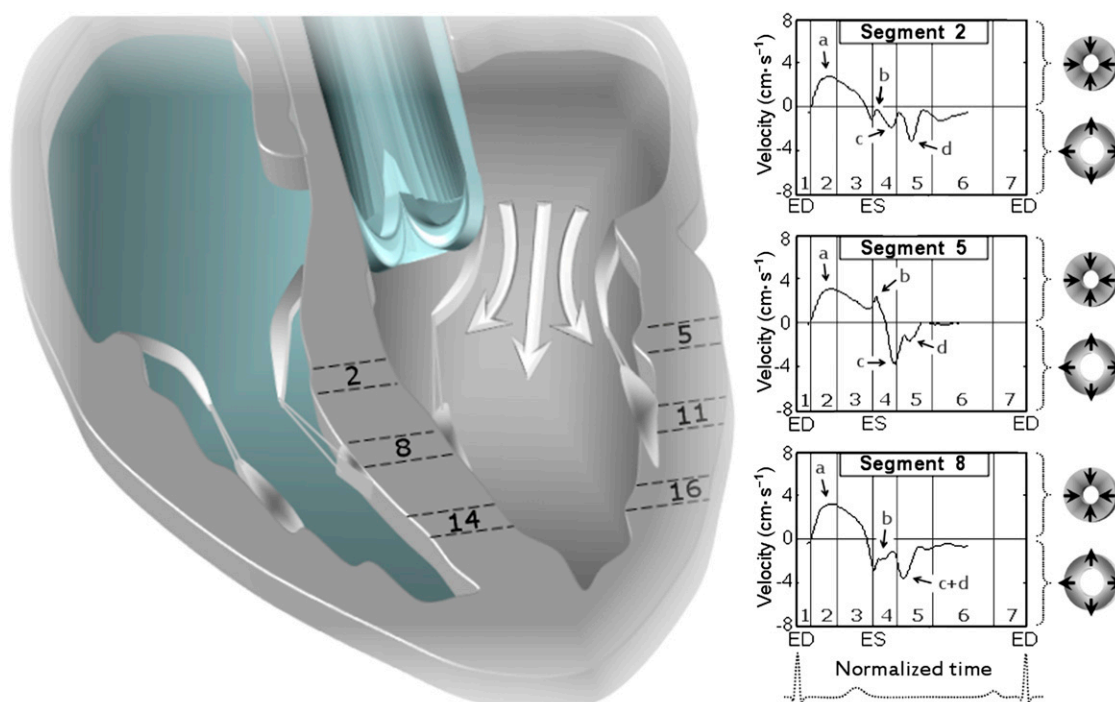
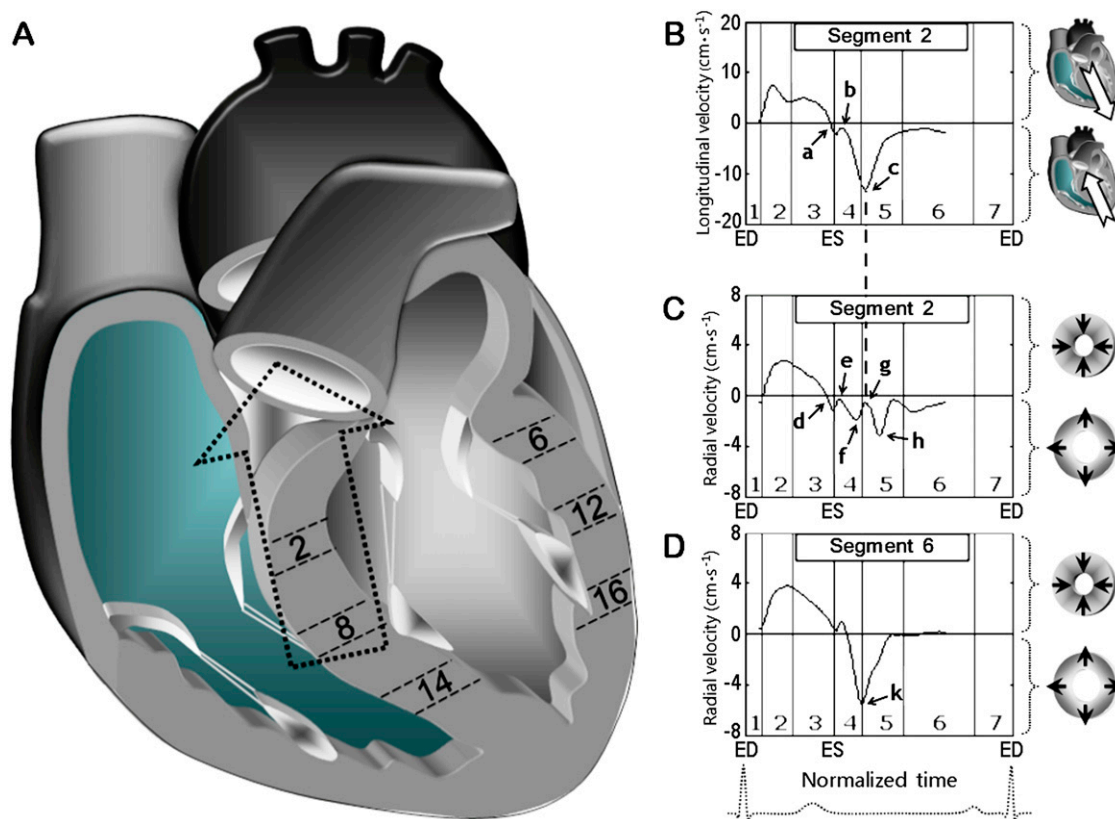


Figure 6. Schematic representation of left ventricular segments on the cross-section (A) with simultaneous display of radial (B) and longitudinal (C) velocities of Segment 2. The radial velocity curve of Segment 6 (D) is provided for comparison. The upward displacement of the left ventricle in early diastole by the stretched great vessels and their close apposition to the anterior septum resulted in a biphasic radial expansion of anteroseptal segments (waves f and h). Wave f shows the commencement of radial expansion in early diastole, which gradually decreased as the velocity of the longitudinal motion increased, the lowest velocities of radial expansion (arrow g) corresponding to the highest velocities of upward longitudinal displacement (arrow c). Subsequently, as the velocity of upward longitudinal motion decreased, a second wave of radial expansion was recorded (wave h). Segments: 2, basal anteroseptal segment; 6, basal anterolateral segment; 8, mid-anteroseptal segment; 12, mid-anterolateral segment; 14, apical septal segment; and 16, apical lateral segment. Cardiac cycle phases: 1, isovolumetric contraction; 2, rapid ejection; 3, reduced ejection; 4, isovolumetric relaxation; 5, rapid filling; 6, diastasis; and 7, atrial systole. ED, end diastole; ES, end systole.



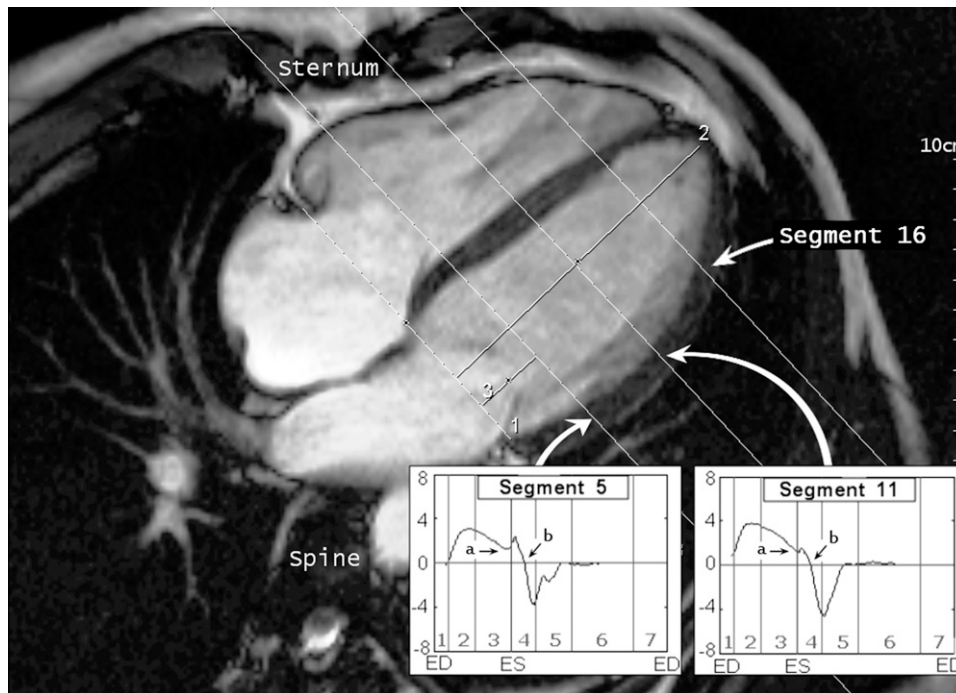
segments, peak systolic velocities were reached during the phase of rapid ejection (Figure 3, wave a), after which the velocity of the inward radial movement gradually decreased until the end of systole, resembling the pattern of corresponding basal LV segments. For example, a delay in the commencement of radial expansion of the mid-inferolateral segment (*i.e.* Segment 11) resembled the pattern recorded in the basal inferolateral segment (*i.e.* Segment 5). The radial velocity curve in these segments remained well above zero at the end of systole at both the LV base and mid-ventricle and showed no outward radial expansion until the second half of isovolumetric relaxation. The biphasic pattern of radial expansion of the mid-anteroseptal segment (*i.e.* Segment 8) was less pronounced than that noted in the basal anteroseptal segment (*i.e.* Segment 2), the two waves of outward radial motion overlapping at the mid-ventricle (Figure 3, Segment 8, waves c and d). The additional wave of outward radial motion during the phase of rapid ventricular filling, corresponding to the expected timing of the third heart sound, was also less prominent at the mid-ventricular level (Figure 3, wave d).

The peak systolic and diastolic radial velocities of mid-ventricular segments are shown in Table 3. The *post hoc* Scheffé test showed significant differences ( $p < 0.05$ ) between peak systolic velocities recorded in the following segments: 8 vs 10 for the inner (endocardial) layer; 7 vs 8; 8 vs 7, 10; 10 vs 8, 12; and 12 vs 10 for both middle (transmural) and outer (epicardial) layers.

#### Radial velocities of apical left ventricular segments

The variation in radial velocities during a cardiac cycle for apical LV segments is shown in Figure 4. Similar to the LV base and mid-ventricle, peak systolic radial velocities were reached during the phase of rapid ejection (Figure 4, wave a), after which the velocity of the inward radial movement gradually decreased until the end of systole. A delay in the commencement of radial expansion was noted in the apical lateral segment (*i.e.* Segment 16), its radial velocity curve remaining above zero at the end of systole and showing no outward radial expansion until the second half of isovolumetric relaxation (Figure 4). The pattern

Figure 7. A representative cardiac MR image showing the positioning of inferolateral segments during the scan. With subjects in the supine position, the heart was “resting” on the inferolateral segments (*i.e.* Segments 5 and 11). This might be responsible for the initial delay in the radial expansion of these segments with a particular shape of their velocity curves, which remained well above zero at the end of systole (arrow a) and showed no outward radial expansion until the second half of isovolumetric relaxation (arrow b). At the left ventricular apex, a similar pattern of radial expansion was recorded for the lateral apical segment (*i.e.* Segment 16), which is also located along the inferior heart surface. Segments: 5, basal inferolateral segment; 11, mid-inferolateral segment; and 16, lateral apical segment. Cardiac cycle phases: 1, isovolumetric contraction; 2, rapid ejection; 3, reduced ejection; 4, isovolumetric relaxation; 5, rapid filling; 6, diastasis; and 7, atrial systole. ED, end diastole; ES, end systole.



resembled that recorded in the inferolateral segments at the LV base and mid-ventricle (*i.e.* Segments 5 and 11).

The peak systolic and diastolic radial velocities for apical LV segments are provided in Table 4. The difference between means estimated by ANOVA did not reach statistical significance (Table 4).

## DISCUSSION

The higher temporal resolution of navigator-gated TPM allowed visualization of new details of LV wall motion. The higher peak systolic radial velocities of the anterior and inferior segments compared with septal and lateral segments recorded at the LV base and mid-ventricle are rather suggestive of a relatively higher dynamics of anteroposterior *vs* lateral LV inward motion. The upright directed notch in early diastole (wave b in Figures 1–4) reflects a brief thrust of inward movement in early diastole (when the notch is above zero) or a sudden deceleration in the radial expansion of the ventricular wall (when the notch is below zero). The notch is synonymous with the notch seen on the aortic pulse wave, corresponding to the expected timing of the reflected pressure wave reaching the left ventricle and has been described elsewhere.<sup>17</sup>

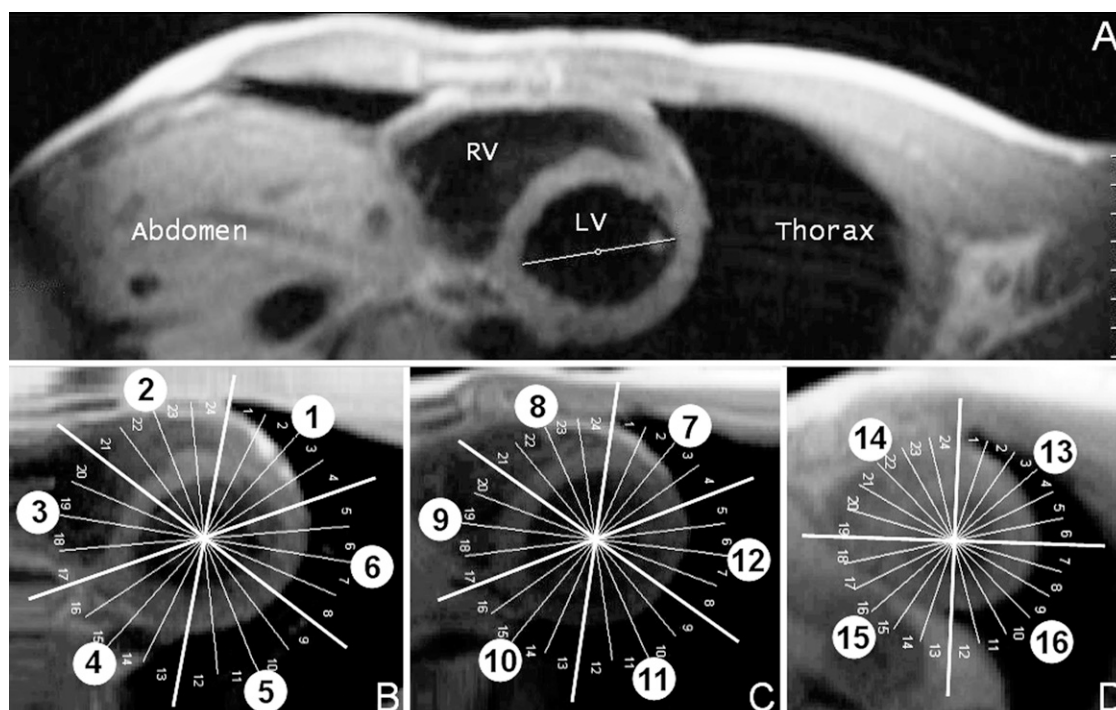
The additional wave of outward radial movement during rapid ventricular filling (wave d in Figures 1–3) corresponds to the

expected timing of the third heart sound. Studies involving mechanical correlations have shown that the third heart sound could be related to ventricular wall vibrations during rapid filling,<sup>18,19</sup> and our results support this hypothesis. A schematic representation of LV segments in the cross-section and their relationship to the direction of ventricular inflow is shown in Figure 5. The septal myocardium and the inferolateral segment (*i.e.* Segment 5) are likely to be particularly influenced by ventricular filling because of the direction of blood flow. The additional wave of outward radial motion we observed was particularly prominent in these segments, further supporting the ventricular theory of the third heart sound.

Another interesting finding was the biphasic radial expansion of Segment 2 (Figure 1, Segment 2, waves c and d). We hypothesize that this can be explained by the simultaneous longitudinal displacement of the left ventricle following repolarization. During systole, the entire ventricle was pushed in an opposite direction to the ejected blood, synonymous to a canon after being fired, stretching the great vessels and elastic structures to which it was attached.<sup>2</sup> After repolarization, the stretched aortic root and pulmonary artery are pulling the ventricular base towards its initial location and this recoil motion may be responsible for the biphasic radial expansion noted in anteroseptal segments. As the basal anteroseptal segment (*i.e.* Segment 2), which is located in immediate proximity to the great vessels, was pulled upwards with



Figure 8. A representative sagittal image (A) and the positioning of basal (B), mid-ventricular (C) and apical (D) segments during the scan. The image confirms the inferior position of Segments 5 and 11, probably causing an initial delay in their radial expansion. Segments: 1, basal anterior segment; 2, basal anteroseptal segment; 3, basal inferoseptal segment; 4, basal inferior segment; 5, basal inferolateral segment; 6, basal anterolateral segment; 7, mid-anterior segment; 8, mid-antерoseptal segment; 9, mid-inferoseptal segment; 10, mid-inferior segment; 11, mid-inferolateral segment; 12, mid-antерolateral segment; 13, apical anterior segment; 14, apical septal segment; 15, apical inferior segment; and 16, apical lateral segment. RV, right ventricle; LV, left ventricle.

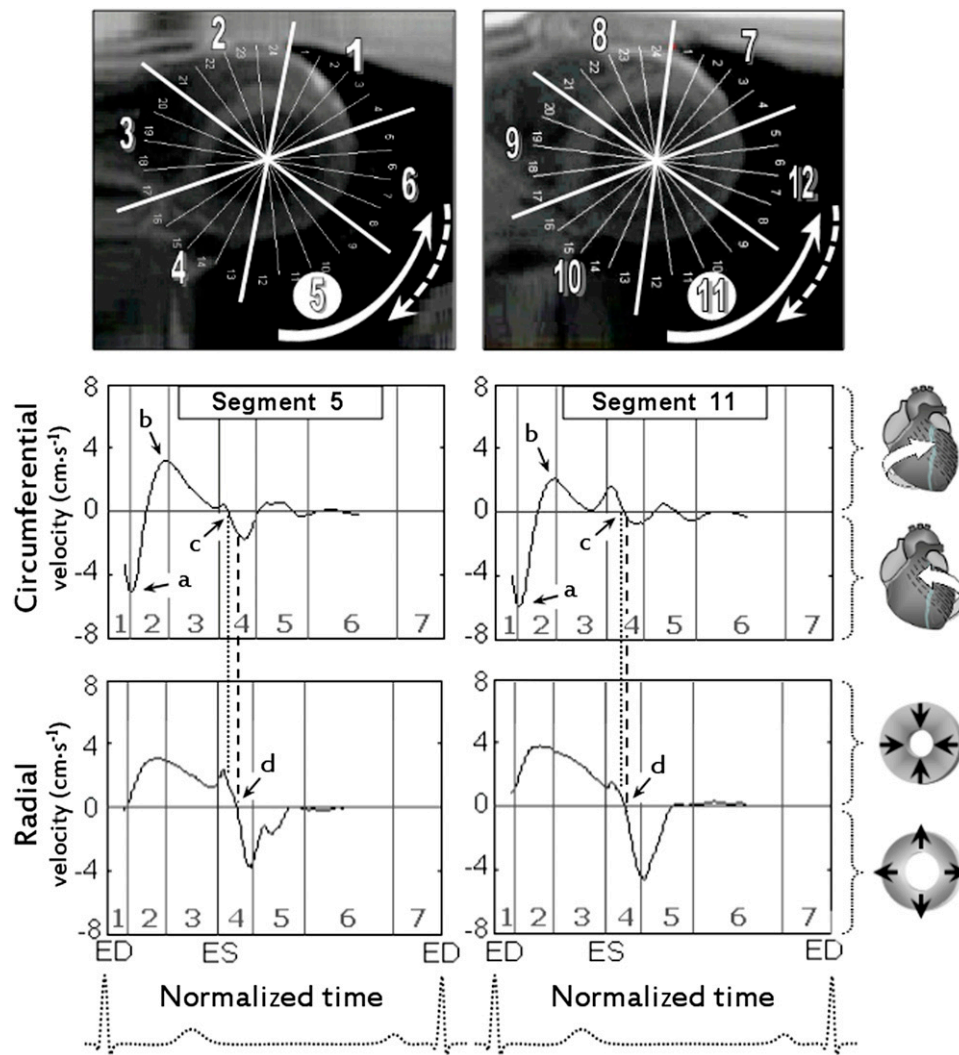


significant force, its radial movement was also affected (Figure 6, panel A). To test this hypothesis, we studied both longitudinal and radial velocities of Segment 2 recorded simultaneously (Figure 6, panels B and C). After repolarization (denoted by the T wave on electrocardiography), Segment 2 started moving upwards and outwards as reflected by negative values on longitudinal and radial velocity graphs (Figure 6, arrows a and d). The upward directed notch at the beginning of diastole shows a brief deceleration in the started upward movement (wave b) and radial expansion (wave e), probably caused by the impact with the reflected pressure wave travelling in the opposite direction.<sup>17</sup> Subsequently, the basal anteroseptal segment (*i.e.* Segment 2) continued its upward movement with increasing velocity over the entire phase of isovolumetric relaxation, reaching peak longitudinal velocities at the beginning of rapid ventricular filling (Figure 6, arrow c). However, as the velocity of its longitudinal motion increased, the velocity of the radial expansion was dropping (Figure 6, curve segment between waves f and g), the lowest velocity values of radial expansion of Segment 2 (Figure 6, arrow g) corresponding to its peak upward longitudinal displacement (Figure 6, arrow c). Although in most ventricular segments outward radial velocities gradually increased during isovolumetric relaxation (Figure 6, wave k), the radial expansion of Segment 2 was minimal at the end of this phase (Figure 6, arrow g). Subsequently, as the velocity of the upward longitudinal displacement decreased, a second wave of radial expansion was recorded (Figure 6, wave h), reflecting a bi-phasic radial expansion in this segment (Figure 6, waves f and h). The radial expansion of the adjacent Segments 8 and 3 was

similarly affected, but to a lesser extent (Figures 2, 3; Segments 3, 8; arrow c). Although this is likely to relate to the recoiled longitudinal pull of the left ventricle towards its initial location, the resulting diastolic wave of outward radial motion of the anteroseptal ventricular wall occurs in the phase of rapid ventricular filling and may also contribute to the mechanism of the third heart sound.

The recorded delay in the commencement of radial expansion of inferolateral segments (*i.e.* Segments 5 and 11) may be related to their positioning during the scan (Figure 7). With subjects in the supine position, the heart was “resting” on the inferolateral segments, directly affecting their radial expansion. A representative sagittal image with delineated LV segments is also shown in Figure 8, which confirms the inferior position of Segments 5 and 11. We hypothesize that this inferior position (with the heart “on top”) could cause an initial delay in the radial expansion of these segments until they rotated in a counterclockwise direction as a result of ventricular untwisting. To explore this hypothesis, we correlated the circumferential and radial velocities of inferolateral segments recorded simultaneously (Figure 9). The graphs confirmed that radial expansion in these segments began only after they rotated in a counterclockwise direction, probably enabling them to “escape” their inferior position. Of note is that the inferolateral segments may also partially “escape” their inferior position in early systole, when the entire ventricle rotates in a counterclockwise direction. During their subsequent clockwise rotation, however, these segments must “lift” the entire heart against gravity to return to their inferior position (Figure 9, dashed

Figure 9. Simultaneous circumferential and radial velocities of Segments 5 and 11. The outward radial expansion was delayed in these segments until they rotated in a counterclockwise direction (as indicated by the white curved arrow), “escaping” their inferior position. Black arrows: a, peak counterclockwise velocity at the beginning of systole; b, peak clockwise velocity during ventricular twisting; c, commencement of counterclockwise rotation during ventricular untwisting; and d, commencement of outward radial expansion. The interval between the dotted and dashed lines represents the period between the commencement of counterclockwise rotation in diastole and the beginning of radial expansion. Of note is that the inferolateral segments may also “escape” at least partially their inferior position in early systole when the entire ventricle rotates in a counterclockwise direction (wave a). During their subsequent clockwise rotation (wave b), however, these segments must “lift” the entire heart against gravity to return to their inferior position (as indicated by the dashed curved arrow). This may represent another contributing factor for the slightly lower peak clockwise velocities of inferolateral segments that we reported previously.<sup>1</sup>



curved arrow). This may represent another contributing factor for the slightly lower peak clockwise velocities of inferolateral segments that we reported previously.<sup>1</sup> Such a limitation in the clockwise rotation of inferolateral segments owing to their inferior positioning is expected to be more pronounced at the LV base (Figure 7), which is also consistent with our previous findings.<sup>1</sup>

#### Study limitations and perspectives

The additional wave of outward radial wall motion corresponding to the expected timing of the third heart sound represents an incidental finding. Although all subjects were young healthy males in whom a third heart sound was expected to be present, no assessment for the presence of the sound was performed before

the study. Assessing regional wall motion findings in a larger range of healthy volunteers and patients with cardiac diseases would help confirm this hypothesis. Correlating the size of this additional wave of outward radial motion with phonocardiographic recordings may provide new information about its diagnostic value and usefulness in clinical practice. Direct velocity measurements could be performed only for the inner (endocardial) and outer (epicardial) layers, which were related to spatial resolution parameters. Transmural peak velocities were inferred automatically as averaged peak values of the inner and outer layers. The myocardial apex segment or apical cap beyond the LV cavity (*i.e.* AHA Segment 17) was not included in the current study. The cardiac phases were calculated and normalized for the entire group based on their

average duration during systole and diastole and not on the timing of cardiac valves closure and opening, which was not recorded. The phases are provided for general orientation and, even when slightly displaced, would not affect data interpretation. New studies with cardiac MR scans performed on healthy subjects in a prone position would confirm our hypothesis related to the particular motion patterns of inferolateral segments.

## CONCLUSIONS

The new details of radial wall motion of individual LV segments obtained using the myocardial velocity-encoding technique provide new insights into the mechanics of the left ventricle. At the LV base and mid-ventricle, the higher peak systolic radial velocities of the anterior and inferior segments are suggestive of a relatively higher dynamics of anteroposterior vs lateral ventricular wall motion in systole. The outward radial movement of

LV segments impacted by the blood flow during rapid ventricular filling provides a potential substrate for the low-frequency brief vibratory sound synonymous with the auscultatory findings of the third heart sound. A biphasic radial expansion of the basal anteroseptal segment is likely to be related to the simultaneous longitudinal displacement of the left ventricle in early diastole by the stretched great vessels and their close apposition to this segment. This biphasic wave of sudden alternating motions may also contribute to the mechanisms of the third heart sound. An initial delay in the radial expansion of inferolateral segments is most likely to be related to their inferior position during the scan.

## FUNDING

This research was funded by the British Heart Foundation and Oxford Partnership Comprehensive Biomedical Research Centre.

## REFERENCES

- Codreanu I, Robson MD, Rider OJ, Pegg TJ, Dasanu CA, Jung BA, et al. Effects of ventricular insertion sites on rotational motion of left ventricular segments studied by cardiac MR. *Br J Radiol* 2013; **86**: 20130326. doi: [10.1259/bjr.20130326](https://doi.org/10.1259/bjr.20130326).
- Codreanu I, Robson MD, Golding SJ, Jung BA, Clarke K, Holloway CJ. Longitudinally and circumferentially directed movements of the left ventricle studied by cardiovascular magnetic resonance phase contrast velocity mapping. *J Cardiovasc Magn Reson* 2010; **12**: 48.
- Zhang H, Zhang Y, Li Z, Liu C, Hou R, Zhu S, et al. Left ventricular radial systolic dysfunction in diabetic patients assessed by myocardial acceleration derived from velocity vector imaging. *J Ultrasound Med* 2012; **31**: 1179–86.
- Maier SE, Fischer SE, McKinnon GC, Hess OM, Krayenbuehl HP, Boesiger P. Evaluation of left ventricular segmental wall motion in hypertrophic cardiomyopathy with myocardial tagging. *Circulation* 1992; **86**: 1919–28.
- Foley PW, Khadjooi K, Ward JA, Smith RE, Stegmann B, Frenneaux MP, et al. Radial dyssynchrony assessed by cardiovascular magnetic resonance in relation to left ventricular function, myocardial scarring and QRS duration in patients with heart failure. *J Cardiovasc Magn Reson* 2009; **11**: 50. doi: [10.1186/1532-429X-11-50](https://doi.org/10.1186/1532-429X-11-50).
- Jung B, Foll D, Bottler P, Petersen S, Hennig J, Markl M. Detailed analysis of myocardial motion in volunteers and patients using high-temporal-resolution MR tissue phase mapping. *J Magn Reson Imaging* 2006; **24**: 1033–9. doi: [10.1002/jmri.20703](https://doi.org/10.1002/jmri.20703)
- Jung B, Markl M, Foll D, Hennig J. Investigating myocardial motion by MRI using tissue phase mapping. *Eur J Cardiothorac Surg* 2006; **29**(Suppl. 1): S150–7. doi: [10.1016/j.ejcts.2006.02.066](https://doi.org/10.1016/j.ejcts.2006.02.066)
- Davidsen ES, Moen CA, Matre K. Radial deformation by tissue Doppler imaging in multiple myocardial layers. *Scand Cardiovasc J* 2010; **44**: 82–91. doi: [10.1080/14017430903177708](https://doi.org/10.1080/14017430903177708)
- Rosner A, How OJ, Aarsaether E, Stenberg TA, Andreassen T, Kondratiev TV, et al. High resolution speckle tracking dobutamine stress echocardiography reveals heterogeneous responses in different myocardial layers: implication for viability assessments. *J Am Soc Echocardiogr* 2010; **23**: 439–47.
- Matre K, Moen CA, Fanelop T, Dahle GO, Grong K. Multilayer radial systolic strain can identify subendocardial ischemia: an experimental tissue Doppler imaging study of the porcine left ventricular wall. *Eur J Echocardiogr* 2007; **8**: 420–30. doi: [10.1016/j.euje.2007.03.031](https://doi.org/10.1016/j.euje.2007.03.031)
- Moen CA, Salminen PR, Grong K, Matre K. Left ventricular strain, rotation, and torsion as markers of acute myocardial ischemia. *Am J Physiol Heart Circ Physiol* 2011; **300**: H2142–54. doi: [10.1152/ajpheart.01012.2010](https://doi.org/10.1152/ajpheart.01012.2010)
- Becker M, Ocklenburg C, Altiok E, Futing A, Balzer J, Krombach G, et al. Impact of infarct transmural on layer-specific impairment of myocardial function: a myocardial deformation imaging study. *Eur Heart J* 2009; **30**: 1467–76. doi: [10.1093/eurheartj/ehp112](https://doi.org/10.1093/eurheartj/ehp112)
- Bachner-Hinenzon N, Ertracht O, Leitman M, Vered Z, Shimoni S, Beerl R, et al. Layer-specific strain analysis by speckle tracking echocardiography reveals differences in left ventricular function between rats and humans. *Am J Physiol Heart Circ Physiol* 2010; **299**: H664–672.
- Codreanu I, Pegg TJ, Selvanayagam JB, Robson MD, Rider OJ, Dasanu CA, et al. Details of left ventricular remodeling and the mechanism of paradoxical ventricular septal motion after coronary artery bypass graft surgery. *J Invasive Cardiol* 2011; **23**: 276–82.
- Codreanu I, Pegg TJ, Selvanayagam JB, Robson MD, Rider OJ, Dasanu CA, et al. Normal values of regional and global myocardial wall motion in young and elderly individuals using navigator gated tissue phase mapping. *Age (Dordr)* 2014; **36**: 231–41.
- Cerqueira MD, Weissman NJ, Dilsizian V, Jacobs AK, Kaul S, Laskey WK, et al. Standardized myocardial segmentation and nomenclature for tomographic imaging of the heart. A statement for healthcare professionals from the Cardiac Imaging Committee of the Council on Clinical Cardiology of the American Heart Association. *Circulation* 2002; **105**: 539–42.
- Codreanu I, Robson MD, Rider OJ, Pegg TJ, Jung BA, Dasanu CA, et al. Chasing the reflected wave back into the heart: a new hypothesis while the jury is still out. *Vasc Health Risk Manag* 2011; **7**: 365–73. doi: [10.2147/VHRM.S20845](https://doi.org/10.2147/VHRM.S20845)
- Glower DD, Murrah RL, Olsen CO, Davis JW, Rankin JS. Mechanical correlates of the third heart sound. *J Am Coll Cardiol* 1992; **19**: 450–7.
- Longhini C, Scorzoni D, Baracca E, Brunazzi MC, Chirillo F, Fratti D, et al. The mechanism of the physiologic disappearance of the third heart sound with aging. *Jpn Heart J* 1996; **37**: 215–26.